THE JOURNAL OF PHYSICAL CHEMISTRY Letters

Letter

Cite This: J. Phys. Chem. Lett. 2019, 10, 5687−5693

pubs.acs.org/JPCL

Direct−Indirect Transition of Pressurized Two-Dimensional Halide Perovskite: Role of Benzene Ring Stack Ordering

Chaofeng Gao,[†,#] Ruiping Li,[†,#] Yiran Li,[†] Rong Wang,[†] Meng Wang,[†] Zhixing Gan,[‡] Ligang Bai,[§] Yucheng Liu,[∥] Kui Zhao,[∥] Shengzhong Frank Liu,[∥] Yingchun Cheng,*[,†] and Wei Huang*[,†,⊥]

[†]Key Laboratory of Flexible Electronics & Institute of Advanced Materials, Jiangsu National Synergetic Innovation Center for Advanced Materials, Nanjing Tech University, 30 South Puzhu Road, Nanjing 211816, China

[‡]Jiangsu Key Laboratory of Optoelectronic Technology, School of Physics and Technology, Nanjing Normal University, Nanjing 210023, China

[§]Institute of High Energy Physics, Chinese Academy of Sciences, Beijing 100049, China

[∥]Key Laboratory of Applied Surface and Colloid Chemistry, Ministry of Education, Shaanxi Key Laboratory for Advanced Energy Devices, Shaanxi Engineering Lab for Advanced Energy Technology, School of Materials Science and Engineering, Shaanxi Normal University, Xi'an 710119, P.R. China

[⊥]Shaanxi Institute of Flexible Electronics (SIFE), Northwestern Polytechnical University (NPU), 127 West Youyi Road, Xi'an, 710072 Shaanxi, China

Supporting Information

ABSTRACT: Two-dimensional (2D) hybrid organic−inorganic metal halide perovskites (HOIPs) with considerably hydrophobic phenyl ethylammonium (PEA) organic cations have been used in highly efficient solar cells and LEDs, which are stable and enjoy a long lifetime, even when exposed to moisture. Different from other 2D HOIPs with alkyl amine cations, a benzene ring is present in the PEA cation. Until recently, an understanding of the effects of PEA on the structural, electronic, and optical properties of 2D HOIPs under pressure has remained limited. We find that there is a direct−indirect band gap transition at around 5.8 GPa and that the direct band gap recovers when the pressure is released. The stacking order of the benzene rings in the PEA cation plays a critical role in the mechanical and electronic properties. Our present work demonstrates that 2D HOIPs with organic cations containing benzene rings prove highly attractive for use in flexible optoelectronics.

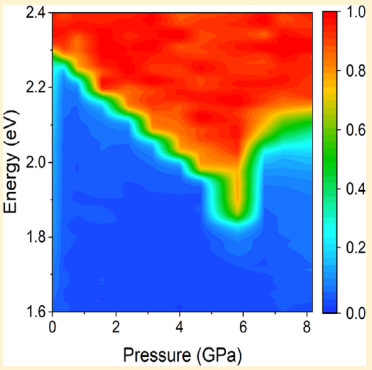

Two-dimensional (2D) hybrid organic−inorganic metal halide perovskites (HOIPs) have a sandwich structure with alternating organic and inorganic components. The organic component is considered a dielectric layer, and the carriers are confined to the inorganic component. Because the inorganic component is atomically thin, the exciton binding energy is very large, which leads to quite efficient radiative recombination. 2D HOIPs, therefore, hold great promise for light-emitting diode (LED) applications.[1−3] The general formula of 2D HOIPs is $(RNH_3)_2MX_4$, where R is an alkyl or aromatic moiety, M a metal cation, and X a halogen atom.[4] Different choices of R group will lead to different 2D HOIPs with different layer−layer distances, binding energies, and stabilities.[5,6] Phenyl ethylammonium (PEA) has been used to synthesize 2D HOIPs for the construction of highly efficient solar cells[7,8] and LEDs.[9,10] Moreover, because of the high hydrophobicity of the PEA^+ cation, optoelectronic devices based on PEA 2D HOIPs exhibit high stability and long lifetimes when suffering light and moisture exposure, indicating their bright prospects in applications that suffer the same.[11,12]

With the development of flexible electronics and HOIPs, it has been demonstrated that HOIPs possess great promise in the construction of flexible solar cells[13,14] and flexible LEDs.[15−17] In the practical applications of flexible devices, the essential tensile and compressive strain on the functional material is very important.[18,19] In addition, even for traditional electronics, device performance and stability are also important under extreme conditions, such as high pressure.[20,21] Therefore, the study of the structural, electronic, and optical properties of 2D HOIPs under high pressure is important, not only in practical terms, but also in the context of obtaining a fundamental understanding of structure−property relations. There are various high-pressure studies of three-dimensional HOIPs, such as $MAPbI_3$,[22−26] $HC(NH_2)PbI_3$,[27] $CH_3NH_3SnI_3$,[28] $CH_3NH_3PbBr_3$,[29] and $FAPbBr_3$.[30] However, very few studies have been reported on 2D HOIPs, such as $(PEA)_2PbBr_4$,[31] $(BA)_2PbI_4$,[32] and $(NMA)_2PbCl_4$.[33]

In this work, we study the electronic and optical properties of 2D halide perovskite with PEA under high pressures of up to

Received: September 5, 2019
Accepted: September 8, 2019
Published: September 8, 2019

Downloaded via UNIV OF GOTHENBURG on October 24, 2019 at 14:29:07 (UTC).
See https://pubs.acs.org/sharingguidelines for options on how to legitimately share published articles.

© 2019 American Chemical Society

DOI: 10.1021/acs.jpclett.9b02604
J. Phys. Chem. Lett. 2019, 10, 5687−5693

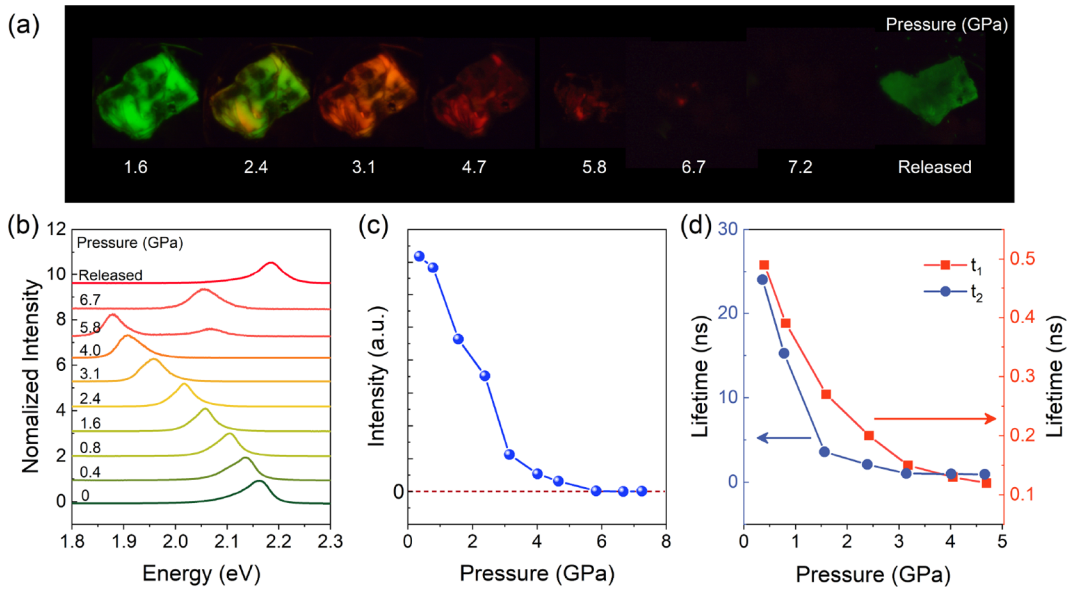

Figure 1. Fluorescent images, PL spectra, and PL lifetime of $(PEA)_2PbI_4$ under high pressure. (a) Fluorescent image of one $(PEA)_2PbI_4$ sample under a series of pressures. (b) PL spectra of $(PEA)_2PbI_4$ under various high pressures. All spectra are normalized. (c) Pressure-dependent PL intensity evolution of $(PEA)_2PbI_4$. (d) PL lifetime under pressure from 0 to 4.7 GPa.

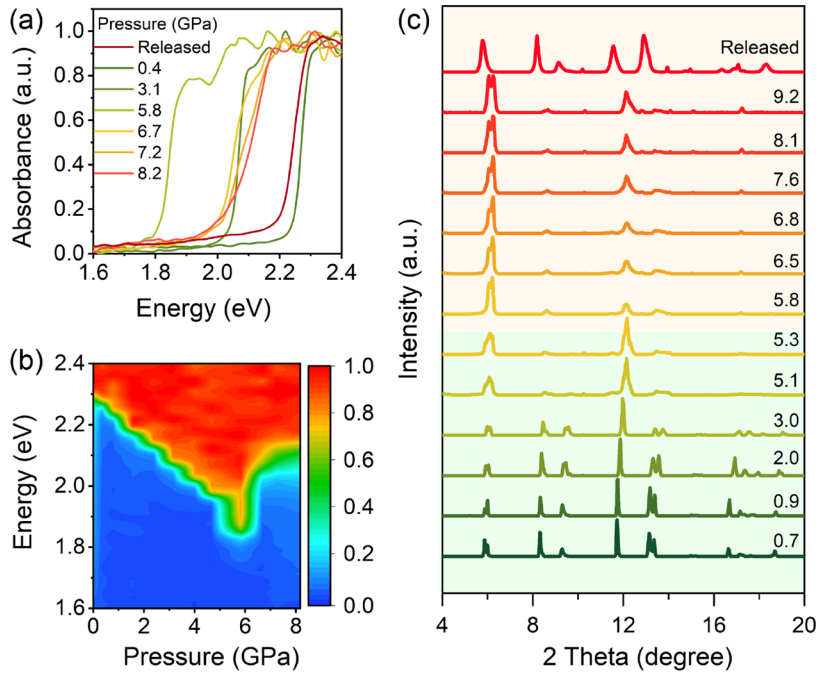

Figure 2. Optical absorption spectra and synchrotron XRD patterns of $(PEA)_2PbI_4$ under high pressure. (a) Optical absorption spectra of $(PEA)_2PbI_4$ during compression and decompression at different pressures. (b) Color map of absorption during compression. (c) Synchrotron XRD patterns of $(PEA)_2PbI_4$ under compression of up to 9.2 GPa and ambient conditions after pressure release.

10 GPa by combining experimental and first-principles calculations. A direct−indirect band gap transition at around 5.8 GPa was found. The direct band gap recovers when pressure is released, indicating a high structural reversibility of $(PEA)_2PbI_4$ under high pressure, which depends critically on the stacking order of the benzene rings. This work demonstrates that 2D HOIPs with organic cations containing benzene rings are highly attractive for use in flexible optoelectronics.

Figure 1 shows the optical properties of $(PEA)_2PbI_4$ under high pressure. The single-crystalline $(PEA)_2PbI_4$ is grown by using a method reported previously.[34] Figure 1a shows that the emission color of $(PEA)_2PbI_4$ changes from green to red, and the intensity decreases with increasing pressure, up to 10 GPa. After the pressure releases, the emission color goes back to green with decreasing intensity. Figure 1b shows normalized photoluminescence (PL) spectra under hydrostatic pressures of up to 6.7 GPa. We observed that the PL peak of $(PEA)_2PbI_4$ shows a clear redshift with increasing pressure. The ambient sample exhibits a green emission centered on 2.16 eV. At low pressure, the PL emission peak shifts slightly toward longer wavelengths, and the emission changes from green to red. At

DOI: 10.1021/acs.jpclett.9b02604
J. Phys. Chem. Lett. 2019, 10, 5687−5693

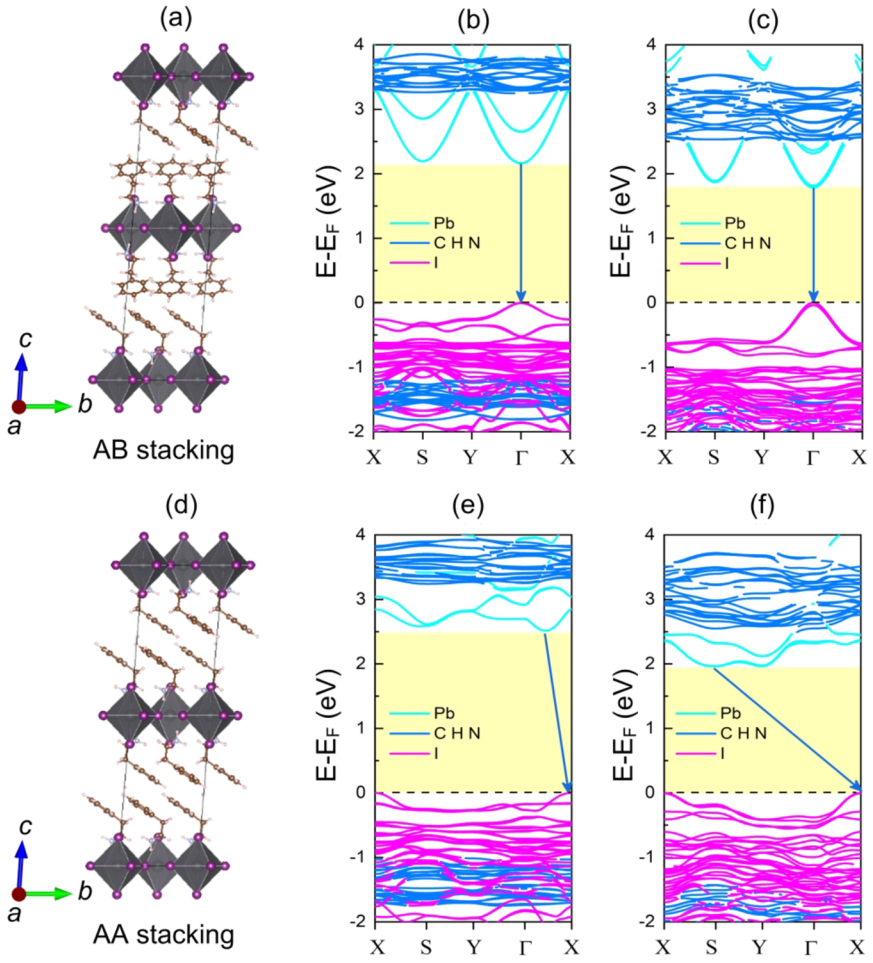

Figure 3. Crystal structures and atom-projected band structure of $(PEA)_2PbI_4$. The crystal structures of (a) AB stacking and (d) AA stacking $(PEA)_2PbI_4$. Band structures of AB stacking under (b) 0 GPa and (c) 7 GPa. Band structures of AA stacking under (e) 0 GPa and (f) 7 GPa. Cyan, magenta, and blue colors represent orbitals from Pb atoms, I atoms, and (C, H, N) groups, respectively. For a specific band, if the orbital contribution from a specific atom or group is larger than 0.7, the band with color is present; otherwise, it is omitted.

5.8 GPa, the emission becomes very weak, and a new peak at 2.07 eV appears. The dual peaks suggest the existence of two phases, implying a possible phase transition at around 5.8 GPa. With further increasing pressure, i.e. up to 6.7 GPa, only the new peak at 2.07 eV is observed, indicating that $(PEA)_2PbI_4$ completely transits to a new phase. After the return to ambient pressure, the PL emission peak returns to that before pressurization.

The PL intensity of the emission decreases with the increase in pressure, as shown in Figure 1c. With a further pressure increment, the luminescence becomes weaker and gradually disappears at 7.2 GPa. After pressure release occurs, the energy of the emission peak returns to 2.18 eV, and the emission color returns to green. However, because the crystalline structure is not fully recovered after pressure release, the PL emission intensity is weaker than that under low pressure, e.g. 1.6 GPa.

Changes in crystal structures may also alter carrier properties, explored by in situ time-resolved photoluminescence (TRPL), shown in Figure 1d. The fluorescence of $(PEA)_2PbI_4$ under higher pressure was too weak and the single-photon signals were too difficult to integrate to acquire PL decay curves; therefore, we show only the changes in lifetime under pressure less than 5.0 GPa. All the PL decay curves are well-fitted by biexponential functions with two lifetime parameters. The fast decay channel (t_1 = 0.49 ns) refers to defect trapping, while the slow decay channel (t_2 = 24 ns) refers to radiative recombination.[35,36] With increasing pressure, the lifetimes of both channels are reduced. Significant shortening of the lifetime for the fast decay channel can be attributed to the increasing defects induced by high pressure. Moreover, the proportion of the slow decay channel is markedly reduced, and the longer lifetime almost vanishes when the pressure rises to 2.4 GPa. The intensity of luminescence decreases with increasing pressure, which is consistent with the changes in the slow decay proportion.

Absorption spectra under high pressure and ambient pressure after pressure release are shown in Figure 2a. At 0.4 GPa, a steep absorption edge is observed at about 2.25 eV, which gradually redshifts with increasing pressure. The movement of the absorption edge is consistent with the fluorescent color changes from green to red. When the pressure reaches 5.8 GPa, the absorption edge shows an exaggerated blue shift, which implies the emergence of a phase transition (see Figure 2b). In addition, by fitting absorbance with photon energy in Figure S1, we can deduce that it is a direct semiconductor under 0.4 GPa, while indirect under 8.2 GPa. The absorption spectrum after high-pressure release is close to that at 0.4 GPa (see Figure 2a).

Figure 2c shows synchrotron XRD patterns of $(PEA)_2PbI_4$ under compression of up to 9.2 GPa. At 5.8 GPa, the peak at

DOI: 10.1021/acs.jpclett.9b02604
J. Phys. Chem. Lett. 2019, 10, 5687−5693

9.3° disappears. In addition, peaks around 5.87° and 11.72° shift to larger angles with a pressure increase from 0.65 to 5.8 GPa but remain almost unchanged with further increasing pressure. We can also deduce that a structural transformation occurs at 5.8 GPa, because with increasing pressure, broad bands appear in the XRD profile. Because the crystal structure of $(PEA)_2PbI_4$ is built from an inorganic skeleton of PbI_4 and an organic cation of PEA with different bonding strengths, the broad bands can be attributed to the pressure-induced deformation of the PbI_4 skeleton, which has been reported in previous studies on various hybrid perovskites under high pressure.[37] After pressure release, we observed that the XRD peaks restored to that at 0.7 GPa with a slight shift of peak positions. This indicates that the high-pressure phase returns to the original $(PEA)_2PbI_4$ crystalline form with almost identical cell parameters; moreover, the $(PEA)_2PbI_4$ structure is reversible, even under high pressure, up to 9.2 GPa.

From previous research, we can infer that the perovskite structure consists of individual $[PbI_4]^{2-}$ octahedral layers which are separated by a double layer of PEA molecules, resulting in a sandwich structure, as shown Figure 3. There exist two estimated structures of $(PEA)_2PbI_4$: One is AB stacking in which the two adjacent layers $[PbI_4]^{2-}$ octahedron have a 50% shift in the "b" direction, and the orientations of the benzene rings of the adjacent two layers are perpendicular to each other,[38,39] as shown in Figure 3a. The other is AA stacking,[40,41] in which the directions of the benzene rings are parallel (see Figure 3d). Some other stackings are also considered (see Figure S2). According to the enthalpy difference, we can find that AA stacking is the most stable phase under 7 GPa (see Figure S3). We calculate the electronic band structures of the $(PEA)_2PbI_4$ in AB and AA stackings as a function of pressure by using density functional theory (DFT) calculations. Four representative band structures of AB and AA stacking at 0 and 7 GPa are shown in Figure 3b,c,e,f. The AB stacking $(PEA)_2PbI_4$ has a direct band gap of 2.16 eV at 0 GPa. The nature of the direct band gap remains as pressure increases to 10 GPa; for example, the band structure at 7 GPa is shown in Figure 3c. In contrast, the band gap of AA stacking is indirect under high pressure, from 0 to 10 GPa. Figure 3e,f shows the indirect band gap nature of AA stacking $(PEA)_2PbI_4$ at 0 and 7 GPa. Therefore, the electronic phase transition at 5.8 GPa from a direct to an indirect band gap can possibly be attributed to the structural phase transition from AB to AA stacking $(PEA)_2PbI_4$.

To further verify the critical pressure of the phase transition from AB to AA, the enthalpy difference of AA and AB stacking $(PEA)_2PbI_4$ as a function of pressure was calculated and is shown in Figure 4a. It is evident that under the critical pressure of 5.83 GPa, the enthalpy of AA stacking $(PEA)_2PbI_4$ is larger than that of AB. Beyond the critical pressure, the enthalpy of AA is smaller than that of AB, indicating a pressure-induced phase transition from AB to AA. We used the linear part of Tauc plots of the absorption edge to extract the band gap.[42] When the pressure is greater than 5.8 GPa, there is a turning point in the band gap of the experiment, indicating a phase transition. Figure 4b shows the experimental optical direct band gap decreasing from 2.26 to 1.83 eV from 0 to 5.8 GPa and then jumping to 1.95 eV (indirect band gap). With further increasing pressure from 5.8 to 8.0 GPa, the indirect band gap decreases. The theoretical band gaps of AB and AA stacking $(PEA)_2PbI_4$ are calculated to compare with experimental results. Before the phase-transition point, the calculated band

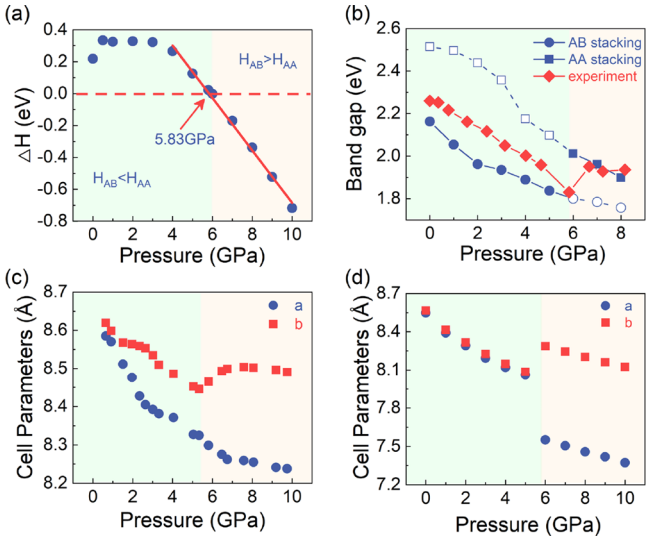

Figure 4. (a) Enthalpy difference of AA and AB stacking $(PEA)_2PbI_4$ under high pressure. (b) Experimental band gap of $(PEA)_2PbI_4$ under high pressure and theoretical band gap of AB and AA stacking $(PEA)_2PbI_4$ under high pressure. (c) Experimental and (d) theoretical lattice parameters under high pressure.

gap of AB stacking decreases with increasing pressure, in good agreement with experiments. The experimental band gap is closer to that of AA stacking with further compression (>5.8 GPa). The value of critical pressure deduced from absorption spectra is also 5.8 GPa.

Figure 4c shows the experimental variations in the lattice constants of *a* and *b*; $(PEA)_2PbI_4$ exhibits anisotropic axial compressibility. At the initial pressure, the value of *a* is close to that of *b*, but with increasing pressure, the difference between *a* and *b* increases. There is an abrupt increase for lattice *a* at around 5.8 GPa, and then *a* decrease. Figure 4d shows the theoretical lattice parameters *a* and *b* for AB and AA stacking $(PEA)_2PbI_4$ as a function of pressure. The lattices *a* and *b* are very close for AB stacking, while they are quite different from each other for AA stacking. When panels c and d of Figure 4 are compared, it is clear that there is a phase transition from AB to AA at the critical pressure of 5.8 GPa.

The structural, electronic, and optical properties of various hybrid perovskites, such as $MAPbI_3$,[43,44] $HC(NH_2)PbI_3$,[27] $CH_3NH_3SnI_3$,[28] $CH_3NH_3PbBr_3$,[29] $FAPbBr_3$,[30] $(PEA)_2PbBr4$,[31] and $(NMA)_2PbCl_4$,[33] have been investigated in recent years. For example, $MAPbX_3$ with high energy conversion efficiency has been considered to be an excellent photovoltaic material. Many studies of $MAPbI_3$ under high pressure have been reported to date. Jaffe et al. reported the pressure effect on the electronic landscapes, excited-state dynamics, and photophysical and transport properties of $MAPbI_3$.[26] Szafrański et al. systematically studied the structure and optical properties of $MAPbI_3$ as a function of pressure.[24] Francisco-López et al. found three structure phase transitions occur in $MAPbI_3$ at 0.4, 2.7, and 3.3 GPa.[25] Wang et al. reported that pressure induced an indirect-to-direct band gap transition in MAPI, and the direct transition lead to a strong light absorption.[22] Most hybrid perovskites undergo an order−disorder phase transition under high pressure. It has been reported that PL spectrum of $(PEA)_2PbBr_4$, a cousin of $(PEA)_2PbI_4$, shows broad peak under high pressure, which is attributed to the deformable $PbBr_4$ skeleton structure.[31]

DOI: 10.1021/acs.jpclett.9b02604
J. Phys. Chem. Lett. 2019, 10, 5687−5693

However, the details of deformation are unknown in this study.[31] In the present work, we found that a stacking-order change from AB to AA under high pressure is responsible for the direct-to-indirect band-structure transformation. One major structural difference between AB and AA stacking is the orientation of the benzene rings in adjacent layers, together with an interlayer shift. In addition, we propose that the benzene ring in the organic cation further enhances the structural reversibility of $(PEA)_2PbI_4$ under high pressure, up to 10 GPa. The benzene ring also exists in $(PEA)_2PbBr_4$, and reversibility is also expected. However, the pressure value in a previous study of $(PEA)_2PbBr_4$ was 28 GPa, which is very large and induces structural destruction.[31]

Though orbital hybridization exists between Pb and I atoms, the highest valence band and lowest conduction band of both stackings at 0 GPa are mainly dominated by orbitals from I and Pb atoms, as shown in panels b and e of Figure 3, respectively. This indicates that the stacking order has only a slight influence on the orbital contribution in the highest valence band and lowest conduction band. At 7 GPa, the occupation of energy states in the highest valence band and lowest conduction band for both stackings is still mainly from the orbitals of I and Pb atoms, respectively (see Figure 3c,f). Though the high pressure does not alter the main orbital contribution in the highest valence band and lowest conduction band, the orbital hybridization between Pb and I atoms is enhanced because of Pb−I bond contraction under high pressure (see Figures S5 and S6). The high pressure also leads to a band gap reduction for both AB and AA stacking $(PEA)_2PbI_4$. The reduction of the band gap originates from the enhanced orbital overlap in the PbI_6 octahedra; therefore, Pb−I bond contraction in PbI_6 octahedra is not responsible for the direct-to-indirect band gap transition.

Stacking order is a critical factor in determining the electronic and optical properties of 2D van der Waals materials. However, there is no reordering of stacking reported in other 2D HOIPs under high pressure, such as $(C_4H_9NH_3)_2PbI_4$.[31] Here, we demonstrate that high pressure induces not only bond-length contraction but also the stacking-order variation in $(PEA)_2PbI_4$. PEA behaves as a spring, which can restore its original structure after pressure release. The benzene ring in PEA plays a critical role in the stacking order transition from AB to AA under high pressure, and it therefore can be viewed as another factor in the tunability of the electronic and optical properties of $(PEA)_2PbI_4$.

In summary, the structural, electronic, and optical properties of 2D HOIP $(PEA)_2PbI_4$ under high pressure, up to 10 GPa, have been investigated. First, we confirmed that the stacking order of $(PEA)_2PbI_4$ is AB stacking with a direct band gap, in ambient conditions. Second, the color of PL can be tuned from green to red under high pressure because of band gap narrowing. Third, a direct−indirect band gap transition at around 5.8 GPa has been revealed by absorption and PL spectra. The high-pressure phase with the indirect band gap is attributed to AA stacking $(PEA)_2PbI_4$ based on XRD and first-principles calculations. Fourth, $(PEA)_2PbI_4$ recovers an AB stacking order with a direct band gap when pressure is released. The benzene ring plays a critical role in the structural reversibility of $(PEA)_2PbI_4$ under high pressure. This work demonstrates that 2D HOIPs with organic cations containing benzene rings are highly attractive candidates for flexible optoelectronic applications.

METHODS

All calculations used the Quantum ESPRESSO code[45] based on density functional theory (DFT). To correct the London dispersion van der Waals interaction, the DFT-D2 approach of Grimme[46] was applied. The Perdew−Burke−Ernzerhof parametrized generalized gradient approximation[47] was used as the exchange−correlation potential. The plane-wave cutoff was set to 544 eV, and a $2 \times 2 \times 1$ k mesh sampling was applied. All the structures were relaxed until the force on each atom was minimized below 1.94×10^{-5} eV/Å.

A diamond anvil cell (DAC) with a 0.4 mm diamond culet was used for generating high pressure in the experiments (see Figure S4). The $(PEA)_2PbI_4$ sample and the ruby were loaded into a 0.14 mm diameter aperture, which was drilled in the center of the preindented T301 gasket. Silicon oil was used as a pressure-transmitting medium. Ruby fluorescence was applied to calibrate the pressure value. All experiments were conducted in ambient conditions.

An Ocean Optics QE65000 scientific-grade spectrometer was applied for absorption signal detection. The absorption spectra were measured based on the transmittance method. Both the fluorescence spectra and absorption spectra were collected with a Princeton Instruments HRS300 spectrometer and an Andor DU970 EMCCD instrument. The fluorescence spectra were measured with a Metatest Scanpro laser scanning microscope equipped with a 488 nm laser. The fluorescence pictures were taken on an Olympus BX53 microscope. The light source for the absorption spectra was a halogen lamp, and the light source for the fluorescence picture was a high-power 450 nm LED.

ADXRD (angle dispersive X-ray diffraction) measurements were conducted on the 4W2 beamline at the High-Pressure Station of the Beijing Synchrotron Radiation Facility (BSRF) using an image plate area detector (Mar345) and focused beam size of 20×30 μm^2. CeO_2 was chosen as the standard for geometrical calibration. Bragg diffraction rings were converted into plots of intensity versus 2θ using the free software Fit2D.[48]

ASSOCIATED CONTENT

Supporting Information

The Supporting Information is available free of charge on the ACS Publications website at DOI: 10.1021/acs.jpclett.9b02604.

Optical absorption spectra of $(PEA)_2PbI_4$, structures and enthalpy of proposed different stacking of $(PEA)_2PbI_4$, schematic of DAC setup for high-pressure experiment, and atomic orbital projected band structures of $(PEA)_2PbI_4$ (PDF)

AUTHOR INFORMATION

Corresponding Authors

*E-mail: iamyccheng@njtech.edu.cn.
*E-mail: iamwhuang@njtech.edu.cn.

ORCID

Zhixing Gan: 0000-0001-5610-0287
Kui Zhao: 0000-0002-9512-0405
Shengzhong Frank Liu: 0000-0002-6338-852X
Yingchun Cheng: 0000-0002-8495-9184
Wei Huang: 0000-0001-7004-6408

DOI: 10.1021/acs.jpclett.9b02604
J. Phys. Chem. Lett. 2019, 10, 5687−5693

Author Contributions

[#]C.G. and R.L. contributed equally.

Notes

The authors declare no competing financial interest.

■ ACKNOWLEDGMENTS

This work was supported by the National Natural Science Foundation of China (Nos. 61575094, 91733302, and 91833302), National Basic Research Program of China (973 Program, No. 2015CB932200), and Primary Research & Development Plan of Jiangsu Province (BE2016770). This work was also sponsored by the Jiangsu Specially-Appointed Professor programme. We are grateful to the High Performance Computing Center of Nanjing Tech University for supporting the computational resources.

■ REFERENCES

(1) Wang, J.; Wang, N.; Jin, Y.; Si, J.; Tan, Z.-K.; Du, H.; Cheng, L.; Dai, X.; Bai, S.; He, H.; et al. Interfacial Control Toward Efficient and Low-Voltage Perovskite Light-Emitting Diodes. *Adv. Mater.* **2015**, *27*, 2311−2316.

(2) Yuan, M.; Quan, L. N.; Comin, R.; Walters, G.; Sabatini, R.; Voznyy, O.; Hoogland, S.; Zhao, Y.; Beauregard, E. M.; Kanjanaboos, P.; et al. Perovskite Energy Funnels for Efficient Light-Emitting Diodes. *Nat. Nanotechnol.* **2016**, *11*, 872−877.

(3) Wei, Y.; Chu, H.; Tian, Y.; Chen, B.; Wu, K.; Wang, J.; Yang, X.; Cai, B.; Zhang, Y.; Zhao, J. Reverse-Graded 2D Ruddlesden−Popper Perovskites for Efficient Air-Stable Solar Cells. *Adv. Energy Mater.* **2019**, *9*, 1900612.

(4) Dou, L.; Wong, A. B.; Yu, Y.; Lai, M.; Kornienko, N.; Eaton, S. W.; Fu, A.; Bischak, C. G.; Ma, J.; Ding, T.; et al. Atomically Thin Two-Dimensional Organic-Inorganic Hybrid Perovskites. *Science* **2015**, *349*, 1518−1521.

(5) Safdari, M.; Svensson, P. H.; Hoang, M. T.; Oh, I.; Kloo, L.; Gardner, J. M. Layered 2D Alkyldiammonium Lead Iodide Perovskites: Synthesis, Characterization, and Use in Solar Cells. *J. Mater. Chem. A* **2016**, *4*, 15638−15646.

(6) Mao, L.; Tsai, H.; Nie, W.; Ma, L.; Im, J.; Stoumpos, C. C.; Malliakas, C. D.; Hao, F.; Wasielewski, M. R.; Mohite, A. D.; et al. Role of Organic Counterion in Lead- and Tin-Based Two-Dimensional Semiconducting Iodide Perovskites and Application in Planar Solar Cells. *Chem. Mater.* **2016**, *28*, 7781−7792.

(7) Cohen, B.-E.; Wierzbowska, M.; Etgar, L. High Efficiency Quasi 2D Lead Bromide Perovskite Solar Cells Using Various Barrier Molecules. *Sustainable Energy Fuels* **2017**, *1*, 1935−1943.

(8) Cohen, B.-E.; Wierzbowska, M.; Etgar, L. High Efficiency and High Open Circuit Voltage in Quasi 2D Perovskite Based Solar Cells. *Adv. Funct. Mater.* **2017**, *27*, 1604733.

(9) Yang, S.; Niu, W.; Wang, A.-L.; Fan, Z.; Chen, B.; Tan, C.; Lu, Q.; Zhang, H. Ultrathin Two-Dimensional Organic-Inorganic Hybrid Perovskite Nanosheets with Bright, Tunable Photoluminescence and High Stability. *Angew. Chem., Int. Ed.* **2017**, *56*, 4252−4255.

(10) Liang, D.; Peng, Y.; Fu, Y.; Shearer, M. J.; Zhang, J.; Zhai, J.; Zhang, Y.; Hamers, R. J.; Andrew, T. L.; Jin, S. Color-Pure Violet-Light-Emitting Diodes Based on Layered Lead Halide Perovskite Nanoplates. *ACS Nano* **2016**, *10*, 6897−6904.

(11) Byun, J.; Cho, H.; Wolf, C.; Jang, M.; Sadhanala, A.; Friend, R. H.; Yang, H.; Lee, T.-W. Efficient Visible Quasi-2D Perovskite Light-Emitting Diodes. *Adv. Mater.* **2016**, *28*, 7515−7520.

(12) Quan, L. N.; Yuan, M.; Comin, R.; Voznyy, O.; Beauregard, E. M.; Hoogland, S.; Buin, A.; Kirmani, A. R.; Zhao, K.; Amassian, A.; et al. Ligand-Stabilized Reduced-Dimensionality Perovskites. *J. Am. Chem. Soc.* **2016**, *138*, 2649−2655.

(13) Li, L.; Zhang, S.; Yang, Z.; Berthold, E. E. S.; Chen, W. Recent Advances of Flexible Perovskite Solar Cells. *J. Energy Chem.* **2018**, *27*, 673−689.

(14) Yang, D.; Yang, R.; Priya, S.; Liu, S. F. Recent Advances in Flexible Perovskite Solar Cells: Fabrication and Applications. *Angew. Chem., Int. Ed.* **2019**, *58*, 4466−4483.

(15) Lee, S. Y.; Kim, S. H.; Nam, Y. S.; Yu, J. C.; Lee, S.; Kim, D. B.; Jung, E. D.; Woo, J. H.; Ahn, S. M.; Lee, S.; et al. Flexibility of Semitransparent Perovskite Light-Emitting Diodes Investigated by Tensile Properties of the Perovskite Layer. *Nano Lett.* **2019**, *19*, 971−976.

(16) Zhao, F.; Chen, D.; Chang, S.; Huang, H.; Tong, K.; Xiao, C.; Chou, S.; Zhong, H.; Pei, Q. Highly Flexible Organometal Halide Perovskite Quantum Dot Based Light-Emitting Diodes on a Silver Nanowire−Polymer Composite Electrode. *J. Mater. Chem. C* **2017**, *5*, 531−538.

(17) Liu, Y.-F.; Feng, J.; Bi, Y.-G.; Yin, D.; Sun, H.-B. Recent Developments in Flexible Organic Light-Emitting Devices. *Adv. Mater. Technol.* **2019**, *4*, 1800371.

(18) Feng, J. Mechanical Properties of Hybrid Organic-Inorganic CH3NH3BX3 (B = Sn, Pb; X = Br, I) Perovskites for Solar Cell Absorbers. *APL Mater.* **2014**, *2*, 081801.

(19) Tu, Q.; Spanopoulos, I.; Hao, S.; Wolverton, C.; Kanatzidis, M. G.; Shekhawat, G. S.; Dravid, V. P. Out-of-Plane Mechanical Properties of 2D Hybrid Organic-Inorganic Perovskites by Nanoindentation. *ACS Appl. Mater. Interfaces* **2018**, *10*, 22167−22173.

(20) Li, Q.; Zhang, L.; Chen, Z.; Quan, Z. Metal Halide Perovskites under Compression. *J. Mater. Chem. A* **2019**, *7*, 16089−16108.

(21) Li, Q.; Wang, Y.; Pan, W.; Yang, W.; Zou, B.; Tang, J.; Quan, Z. High-Pressure Band-Gap Engineering in Lead-Free Cs2AgBiBr6 Double Perovskite. *Angew. Chem., Int. Ed.* **2017**, *56*, 15969−15973.

(22) Wang, T.; Daiber, B.; Frost, J. M.; Mann, S. A.; Garnett, E. C.; Walsh, A.; Ehrler, B. Indirect to Direct Bandgap Transition in Methylammonium Lead Halide Perovskite. *Energy Environ. Sci.* **2017**, *10*, 509−515.

(23) Postorino, P.; Malavasi, L. Pressure-Induced Effects in Organic−Inorganic Hybrid Perovskites. *J. Phys. Chem. Lett.* **2017**, *8*, 2613−2622.

(24) Szafrański, M.; Katrusiak, A. Mechanism of Pressure-Induced Phase Transitions, Amorphization, and Absorption-Edge Shift in Photovoltaic Methylammonium Lead Iodide. *J. Phys. Chem. Lett.* **2016**, *7*, 3458−3466.

(25) Francisco-López, A.; Charles, B.; Weber, O. J.; Alonso, M. I.; Garriga, M.; Campoy-Quiles, M.; Weller, M. T.; Goñi, A. R. Pressure-Induced Locking of Methylammonium Cations Versus Amorphization in Hybrid Lead Iodide Perovskites. *J. Phys. Chem. C* **2018**, *122*, 22073−22082.

(26) Jaffe, A.; Lin, Y.; Karunadasa, H. I. Halide Perovskites under Pressure: Accessing New Properties through Lattice Compression. *ACS Energy Lett.* **2017**, *2*, 1549−1555.

(27) Liu, G.; Kong, L.; Gong, J.; Yang, W.; Mao, H.-k.; Hu, Q.; Liu, Z.; Schaller, R. D.; Zhang, D.; Xu, T. Pressure-Induced Bandgap Optimization in Lead-Based Perovskites with Prolonged Carrier Lifetime and Ambient Retainability. *Adv. Funct. Mater.* **2017**, *27*, 1604208.

(28) Lu, X.; Wang, Y.; Stoumpos, C. C.; Hu, Q.; Guo, X.; Chen, H.; Yang, L.; Smith, J. S.; Yang, W.; Zhao, Y.; et al. Enhanced Structural Stability and Photo Responsiveness of CH3NH3SnI3 Perovskite via Pressure-Induced Amorphization and Recrystallization. *Adv. Mater.* **2016**, *28*, 8663−8668.

(29) Yin, T.; Fang, Y.; Chong, W. K.; Ming, K. T.; Jiang, S.; Li, X.; Kuo, J. L.; Fang, J.; Sum, T. C.; White, T. J.; et al. High-Pressure-Induced Comminution and Recrystallization of CH3NH3PbBr3 Nanocrystals as Large Thin Nanoplates. *Adv. Mater.* **2018**, *30*, 1705017.

(30) Wang, L.; Wang, K.; Zou, B. Pressure-Induced Structural and Optical Properties of Organometal Halide Perovskite-Based Formamidinium Lead Bromide. *J. Phys. Chem. Lett.* **2016**, *7*, 2556−2562.

(31) Zhang, L.; Wu, L.; Wang, K.; Zou, B. Pressure-Induced Broadband Emission of 2D Organic-Inorganic Hybrid Perovskite (C6H5C2H4NH3)2PbBr4. *Adv. Sci. (Weinheim, Ger.)* **2019**, *6*, 1801628.

DOI: 10.1021/acs.jpclett.9b02604
J. Phys. Chem. Lett. 2019, 10, 5687−5693

(32) Yin, T. T.; Liu, B.; Yan, J. X.; Fang, Y. A.; Chen, M. H.; Chong, W. K.; Jiang, S. J.; Kuo, J. L.; Fang, J. Y.; Liang, P.; et al. Pressure-Engineered Structural and Optical Properties of Two Dimensional (C4H9NH3)(2)PbI4 Perovskite Exfoliated nm-Thin Flakes. *J. Am. Chem. Soc.* **2019**, *141*, 1235−1241.
(33) Du, K. Z.; Tu, Q.; Zhang, X.; Han, Q.; Liu, J.; Zauscher, S.; Mitzi, D. B. Two-Dimensional Lead(II) Halide-Based Hybrid Perovskites Templated by Acene Alkylamines: Crystal Structures, Optical Properties, and Piezoelectricity. *Inorg. Chem.* **2017**, *56*, 9291−9302.
(34) Liu, Y. C.; Zhang, Y. X.; Yang, Z.; Ye, H. C.; Feng, J. S.; Xu, Z.; Zhang, X.; Munir, R.; Liu, J.; Zuo, P.; et al. Multi-Inch Single-Crystalline Perovskite Membrane for High-Detectivity Flexible Photosensors. *Nat. Commun.* **2018**, *9*, 5302.
(35) Wu, Y.; Wei, C.; Li, X.; Li, Y.; Qiu, S.; Shen, W.; Cai, B.; Sun, Z.; Yang, D.; Deng, Z.; et al. In Situ Passivation of PbBr64− Octahedra toward Blue Luminescent CsPbBr3 Nanoplatelets with Near 100% Absolute Quantum Yield. *ACS Energy Lett.* **2018**, *3*, 2030−2037.
(36) Wen, X.; Feng, Y.; Huang, S.; Huang, F.; Cheng, Y.-B.; Green, M.; Ho-Baillie, A. Defect Trapping States and Charge Carrier Recombination in Organic−Inorganic Halide Perovskites. *J. Mater. Chem. C* **2016**, *4*, 793−800.
(37) Wang, Y.; Lu, X.; Yang, W.; Wen, T.; Yang, L.; Ren, X.; Wang, L.; Lin, Z.; Zhao, Y. Pressure-Induced Phase Transformation, Reversible Amorphization, and Anomalous Visible Light Response in Organolead Bromide Perovskite. *J. Am. Chem. Soc.* **2015**, *137*, 11144−11149.
(38) Chen, J.; Lee, D.; Park, N. G. Stabilizing the Ag Electrode and Reducing J-V Hysteresis through Suppression of Iodide Migration in Perovskite Solar Cells. *ACS Appl. Mater. Interfaces* **2017**, *9*, 36338−36349.
(39) Fang, H. H.; Yang, J.; Tao, S. X.; Adjokatse, S.; Kamminga, M. E.; Ye, J. T.; Blake, G. R.; Even, J.; Loi, M. A. Unravelling Light-Induced Degradation of Layered Perovskite Crystals and Design of Efficient Encapsulation for Improved Photostability. *Adv. Funct. Mater.* **2018**, *28*, 1800305.
(40) Ma, D. W.; Fu, Y. P.; Dang, L. N.; Zhai, J. Y.; Guzei, I. A.; Jin, S. Single-Crystal Microplates of Two-Dimensional Organic-Inorganic Lead Halide Layered Perovskites for Optoelectronics. *Nano Res.* **2017**, *10*, 2117−2129.
(41) Liu, W. W.; Xing, J.; Zhao, J. X.; Wen, X. L.; Wang, K.; Lu, P. X.; Xiong, Q. H. Giant Two-Photon Absorption and Its Saturation in 2D Organic-Inorganic Perovskite. *Adv. Opt. Mater.* **2017**, *5*, 1601045.
(42) Tauc, J. Optical Properties and Electronic Structure of Amorphous Ge and Si. *Mater. Res. Bull.* **1968**, *3*, 37−46.
(43) Jiang, S.; Fang, Y.; Li, R.; Xiao, H.; Crowley, J.; Wang, C.; White, T. J.; Goddard, W. A., 3rd; Wang, Z.; Baikie, T.; et al. Pressure-Dependent Polymorphism and Band-Gap Tuning of Methylammonium Lead Iodide Perovskite. *Angew. Chem., Int. Ed.* **2016**, *55*, 6540−6544.
(44) Jaffe, A.; Lin, Y.; Beavers, C. M.; Voss, J.; Mao, W. L.; Karunadasa, H. I. High-Pressure Single-Crystal Structures of 3D Lead-Halide Hybrid Perovskites and Pressure Effects on Their Electronic and Optical Properties. *ACS Cent. Sci.* **2016**, *2*, 201−209.
(45) Giannozzi, P.; Baroni, S.; Bonini, N.; Calandra, M.; Car, R.; Cavazzoni, C.; Ceresoli, D.; Chiarotti, G. L.; Cococcioni, M.; Dabo, I.; et al. QUANTUM ESPRESSO: A Modular and Open-Source Software Project for Quantum Simulations of Materials. *J. Phys.: Condens. Matter* **2009**, *21*, 395502.
(46) Grimme, S. Semiempirical GGA-Type Density Functional Constructed with a Long-Range Dispersion Correction. *J. Comput. Chem.* **2006**, *27*, 1787−99.
(47) Perdew, J. P.; Burke, K.; Ernzerhof, M. Generalized Gradient Approximation Made Simple. *Phys. Rev. Lett.* **1996**, *77*, 3865−3868.
(48) Hammersley, A. P. FIT2D: A Multi-Purpose Data Reduction, Analysis and Visualization Program. *J. Appl. Crystallogr.* **2016**, *49*, 646−652.

DOI: 10.1021/acs.jpclett.9b02604
J. Phys. Chem. Lett. 2019, 10, 5687−5693